

Systematically Evaluating DOTATATE and FDG as PET Immuno-Imaging Tracers of Cardiovascular Inflammation

Yohana C. Toner

Icahn School of Medicine at Mount Sinai

Adam A. Ghotbi

Icahn School of Medicine at Mount Sinai

Sonum Naidu

Icahn School of Medicine at Mount Sinai

Ken Sakurai

Icahn School of Medicine at Mount Sinai

Mandy M.T. Leent

Icahn School of Medicine at Mount Sinai

Stefan Jordan

Charité – Universitätsmedizin Berlin, Universität Berlin, Humboldt-Universität zu Berlin

Farideh Ordikhani

Icahn School of Medicine at Mount Sinai

Letizia Amadori

Icahn School of Medicine at Mount Sinai

Alexandros Marios Sofias

Icahn School of Medicine at Mount Sinai

Elizabeth L. Fisher

Icahn School of Medicine at Mount Sinai

Alexander Maier

Icahn School of Medicine at Mount Sinai

Nathaniel Sullivan

Icahn School of Medicine at Mount Sinai

Jazz Munitz

Icahn School of Medicine at Mount Sinai

Max L. Senders

Icahn School of Medicine at Mount Sinai

Christian Mason

Memorial Sloan-Kettering Cancer Center

Thomas Reiner

Memorial Sloan-Kettering Cancer Center

Georgios Soultanidis

Icahn School of Medicine at Mount Sinai

Jason M. Tarkin

University of Cambridge

James H.F. Rudd

University of Cambridge

Chiara Giannarelli

Icahn School of Medicine at Mount Sinai

Jordi Ochando

Icahn School of Medicine at Mount Sinai

Carlos Pérez-Medina

Icahn School of Medicine at Mount Sinai

Andreas Kjaer

Rigshospitalet and University of Copenhagen

Willem J.M. Mulder

Icahn School of Medicine at Mount Sinai

Zahi A. Fayad

Icahn School of Medicine at Mount Sinai

Claudia Calcagno (✉ claudia.mani@niaid.nih.gov)

Icahn School of Medicine at Mount Sinai

Research Article

Keywords: DOTATATE, 18F-FDG, myocardial infarction, atherosclerosis, cardiovascular inflammation.

Posted Date: December 1st, 2021

DOI: <https://doi.org/10.21203/rs.3.rs-1083300/v1>

License:  This work is licensed under a Creative Commons Attribution 4.0 International License.

[Read Full License](#)

Version of Record: A version of this preprint was published at Scientific Reports on April 13th, 2022. See the published version at <https://doi.org/10.1038/s41598-022-09590-2>.

Abstract

The somatostatin receptor 2-binding PET tracer DOTATATE is emerging as an alternative to ^{18}F -FDG to assess cardiovascular inflammation. The strengths and weaknesses of each tracer and their different specificity for inflammatory cells still need to be fully elucidated. In this manuscript, we employed mouse and rabbit animal models of inflammation. In mice, ^{64}Cu -DOTATATE's pharmacokinetics and timed biodistribution were determined in control (C57BL/6) and atherosclerotic (*ApoE*^{-/-}) mice by *ex vivo* gamma counting. *In vivo* PET/CT, combined with *ex vivo* flow cytometry and gamma counting, was used to evaluate the quantification of cardiovascular inflammation by ^{64}Cu -DOTATATE and ^{18}F -FDG and the tracers' cellular specificity in control versus infarcted and atherosclerotic mice. In a translational PET/MRI rabbit study, we then compared DOTATATE labeled with short-lived radioisotope ^{68}Ga and ^{18}F -FDG for the assessment of aortic inflammation, combined with *ex vivo* radiometric assays and near-infrared imaging of macrophage burden. In infarcted mice, *in vivo* ^{64}Cu -DOTATATE PET showed higher differential uptake than ^{18}F -FDG between infarcted and remote myocardium ($p=0.0286$), and with respect to controls ($p=0.0286$; $n=4-6$). In atherosclerotic mice, ^{64}Cu -DOTATATE PET aortic signal, but not ^{18}F -FDG, was higher compared to controls ($p=0.0286$; $n=4$). In both models, ^{64}Cu -DOTATATE demonstrated preferential accumulation in macrophages with respect to other myeloid cells, while ^{18}F -FDG uptake was less cell-specific. The translational rabbit PET/MRI study showed significantly higher aortic accumulation of both ^{68}Ga -DOTATATE and ^{18}F -FDG in atherosclerotic compared to control animals ($p=0.0002$ and $p=0.0159$, respectively; $n=10-32$). In conclusion, we introduce a workflow integrating *in vivo* PET and *ex vivo* immunological and radioactivity counting assays to characterize DOTATATE and ^{18}F -FDG as inflammation tracers in small animal models of cardiovascular disease. Our results support the use of DOTATATE to assess cardiovascular inflammation, as alternative and complement to ^{18}F -FDG. In addition, our study establishes a comprehensive and robust framework for the thorough assessment and comparison of novel and validated PET immuno-tracers in the cardiovascular arena.

Introduction

Cardiovascular disease is the principal cause of morbidity and mortality worldwide ¹. In the past two decades, pre-clinical and clinical studies ²⁻⁶ have uncovered the critical role of inflammation in atherosclerotic plaque formation and in the onset and resolution of cardio- and cerebrovascular events. As the inflammatory response is emerging as a new diagnostic and therapeutic target in cardiovascular disease, quantitative positron emission tomography (PET) inflammation imaging of the heart and vasculature is rapidly gaining momentum.

Originally developed to identify metabolically active tumors, the PET tracer ^{18}F -fluorodeoxyglucose (^{18}F -FDG) is, to date, the most commonly used inflammation tracer in cardiovascular disease and has been widely validated to quantify atherosclerotic plaque inflammation, myocardial viability and inflammation after ischemia ⁷. Nevertheless, there are several limitations associated with the use of ^{18}F -FDG for

cardiovascular inflammation imaging. As a radiolabeled glucose analog, ^{18}F -FDG is not necessarily specific for inflammatory cells. In fact, *in vitro*⁸ and recent *in vivo* studies⁹, indicate that vascular ^{18}F -FDG signal might also derive from cells other than plaque macrophages. For cardiac imaging, high physiological uptake of ^{18}F -FDG in the healthy and remote myocardium makes it challenging to visualize inflammation in the coronaries or in the infarct itself^{10–12}.

To surpass these limitations, alternative, inflammatory cell-specific PET tracers are being actively investigated for use in cardiovascular disease. Among these, the somatostatin receptor type 2 (SSTR2)-binding PET tracers ^{64}Cu -DOTATATE (Detectnet®) and ^{68}Ga -DOTATATE (Netspot®), approved by the FDA to diagnose SSTR2-positive neuroendocrine tumors^{13,14}, have recently gained significant interest for the quantification of cardiovascular inflammation in mouse models of cardiovascular disease¹⁵, in human plaques^{16,17} and, more recently, in myocardial infarction^{18,19}.

In the era of immuno-imaging, it is imperative to be able to systematically investigate the behavior of different PET inflammation tracers and their interactions with immune cells. Towards this goal, we engineered and deployed a highly complementary workflow integrating *in vivo* PET imaging with *ex vivo* assays to thoroughly characterize and compare DOTATATE and ^{18}F -FDG in small animal models of atherosclerosis and myocardial infarction. In mechanistic studies in mice, we labeled DOTATATE with the long half-life radioisotope copper-64 (^{64}Cu , half-life 12.7 hours) to allow thorough *in vivo* and *ex vivo* characterization of the tracer's pharmacokinetics, timed biodistribution, quantification of cardiovascular inflammation and cellular uptake in comparison with ^{18}F -FDG. This work was supplemented by a translational PET/MRI study in atherosclerotic rabbits that compared the quantification of aortic inflammation by gallium-68 (^{68}Ga , half-life 68 minutes)-labeled DOTATATE and ^{18}F -FDG, as validated by near infra-red fluorescence imaging of macrophage burden.

In addition to providing tracer-specific information, our work introduces a rigorous framework for the thorough immunological assessment and comparison of novel and validated PET tracers in the context of cardiovascular inflammation.

Results

Study design

The aim of this study was to establish a rigorous framework to thoroughly characterize and compare DOTATATE and ^{18}F -FDG for the evaluation of cardiovascular inflammation. In mice, DOTATATE was labeled with the long-lived isotope ^{64}Cu to complement *in vivo* PET with extensive *ex vivo* immunological assays, while, in translational PET/MRI rabbit studies, the tracer was labeled with the short-lived isotope ^{68}Ga (Fig. 1A). ^{64}Cu -DOTATATE's pharmacokinetics and timed organ biodistribution were investigated in wild-type C57Bl/6 and atherosclerosis-prone *Apoe*^{-/-} mice by gamma counting (Fig. 1B and Supplementary Fig. S1A). *In vivo* PET/CT, accompanied by *ex vivo* flow cytometry and autoradiography,

was used to characterize the radiotracers' ability to assess cardiovascular inflammation and uptake by immune cells in mouse models of myocardial infarction and atherosclerosis (Fig. 1C and Supplementary Fig. S1B). Translational rabbit experiments were performed on a clinical PET/MRI scanner. Pharmacokinetic and biodistribution profiles were established in control (non-atherosclerotic) and atherosclerotic rabbits by *ex vivo* gamma counting (Fig. 1B and Supplementary Fig. S2A). Atherosclerotic rabbits were imaged with both ^{68}Ga -DOTATATE and ^{18}F -FDG at different time points after Western diet initiation and compared to non-atherosclerotic controls. PET/MR data was validated with *ex vivo* near-infrared imaging of macrophage burden in the aorta (Fig. 1C and Supplementary Fig. S2B).

^{64}Cu -DOTATATE's *in vivo* behavior in mice

In both control and atherosclerotic mice, ^{64}Cu -DOTATATE was rapidly cleared from the blood, with a weighted blood half-life of, respectively, 4.8 and 6.8 minutes (Fig. 2A and Supplementary Table S1). In both groups, separation of blood fractions revealed that most of the tracer was in the plasma, which contained on average 83.4 ± 0.6 and 88.7 ± 0.9 % of the radioactivity at 120 minutes after radiotracer injection, respectively (Fig. 2B). Density gradient separation of blood cells indicated that the tracer was taken up by mononuclear cells at early time-points, with progressive increase in polynuclear accumulation in control and atherosclerotic animals over the 120 minutes after injection (Fig. 2C). In both C57Bl/6 and *ApoE*^{-/-} mice, gamma counting of clearance organs substantiated the fast removal of ^{64}Cu -DOTATATE from the bloodstream. Shortly after injection, kidneys, bladder and liver cleared up most of the tracer. ^{64}Cu -DOTATATE exhibited affinity for organs, such as pancreas, adrenal gland, stomach and intestines (Fig. 2D and Supplementary Fig. S3A; Supplementary Table S2 and S3).

To investigate if ^{64}Cu -DOTATATE would be suitable for use in cardiovascular disease studies, we evaluated myocardial and aortic uptake over time. In atherosclerotic mice median heart signal at 120 minutes was 1.4 (IQR, 1.2-1.4) %ID/g, which was significantly higher compared to 0.7 %ID/g in controls (IQR, 0.7-0.8, $p=0.0159$, Fig. 2E and Supplementary Fig. S3A; Supplementary Table S2 and S3). Two hours after injection, signal in the thoracic aorta was also significantly higher in atherosclerotic compared to control mice with medians of 2.1 (IQR, 2-2.4) and 1 %ID/g, respectively (IQR, 0.7-1.1, $p=0.0079$, Fig. 2F and Supplementary Fig. S3A; Supplementary Table S2 and S3).

^{64}Cu -DOTATATE and ^{18}F -FDG PET imaging of cardiac inflammation in infarcted mice

In vivo PET/CT with either ^{64}Cu -DOTATATE or ^{18}F -FDG was performed in C57Bl/6 mice 3 days after MI to quantify myocardial inflammation (Supplementary Fig. S1B). ^{64}Cu -DOTATATE PET images showed lower uptake throughout the body, particularly in the muscles (Fig. 3A-C), when compared to ^{18}F -FDG (Fig. 3D-F). *In vivo* ^{64}Cu -DOTATATE SUV_{max} was significantly higher in the infarct with median SUV_{max} 1.3 (IQR, 1.2-1.4) compared to both the hearts of control animals (0.6, IQR, 0.5-0.7, $p=0.0286$), and to the remote (non-infarcted) myocardium (0.7, IQR, 0.5-0.8, $p=0.0286$, Fig. 3B), as confirmed by *ex vivo* gamma counting and autoradiography (Fig. 3C and Supplementary Fig. S3B). In contrast, quantification of ^{18}F -

FDG uptake in control and infarcted hearts showed no significant difference (SUV_{max} 3.4, IQR 2.6-3.7 and 4.2, IQR 3.3-4.6, respectively, $p=0.2571$, Fig. 3E). Within the heart of infarcted animals, we observed a difference in ^{18}F -FDG uptake in the infarcted myocardium with median SUV_{max} 4.2 (IQR, 3.3-4.6) when compared to remote myocardium (2.1, IQR, 2-3.8, $p=0.0411$, Fig. 3E)^{20,21}, but these findings could not be confirmed by *ex vivo* gamma counting (Fig. 3F). By autoradiography, the ratio between the signal in infarcted and remote myocardium was approximately 2 for ^{64}Cu -DOTATATE, but close to 1 for ^{18}F -FDG (Supplementary Fig. S3B), indicating better infarct/remote myocardium delineation using ^{64}Cu -DOTATATE. We postulated that these differences may be attributed to ^{64}Cu -DOTATATE's affinity for SSTR2-expressing cells, particularly macrophages.

To verify this hypothesis, we harvested the infarcted myocardium and cell-sorted $CD11b^+CD11c^+F4/80^+$ (macrophages), $CD11b^+$ (myeloid cells excluding macrophages) and $CD11b^-$ (non-myeloid cells) populations after PET imaging (Fig. 3G, Supplementary Fig. S3C and Supplementary Table S4). Cell suspensions were gamma-counted and radiotracer activity was normalized to the number of cells per sample. The ratio of activity in $CD11b^+$ (myeloid) versus $CD11b^-$ (non-myeloid leukocytes) cells was 6-fold higher for ^{64}Cu -DOTATATE compared to ^{18}F -FDG ($p=0.0286$, Fig. 3H), indicating higher accumulation of ^{64}Cu -DOTATATE in the myeloid cell fraction. Within $CD11b^+$ myeloid cells, ^{64}Cu -DOTATATE was found to accumulate 3-fold more in macrophages with respect to ^{18}F -FDG, although these differences did not reach statistical significance ($p=0.0571$, Fig. 3H).

^{64}Cu -DOTATATE and ^{18}F -FDG PET imaging of vascular inflammation in atherosclerotic mice

Encouraged by ^{64}Cu -DOTATATE's macrophage specificity in the heart, we set out to investigate the application of ^{64}Cu -DOTATATE PET imaging in aortic plaques of *ApoE*^{-/-} atherosclerotic mice. *In vivo* PET showed significantly higher ^{64}Cu -DOTATATE SUV_{max} in the ascending aorta of *ApoE*^{-/-} mice with median of 1.1 (IQR, 0.9-1.3) compared to healthy (non-atherosclerotic) C57Bl/6 mice where median SUV_{max} was 0.5 (IQR, 0.5-0.6, $p=0.0286$, Fig. 4A and 4B). This finding was in agreement with the overall trend of *ex vivo* gamma counting, which, however, did not reach statistical significance, with median %ID/g values of 7.4 (IQR, 3.6-9.9) and 3.5 (IQR, 2.7-4, $p=0.2$, Fig. 4C) in atherosclerotic and control mice, respectively. In atherosclerotic mice, *ex vivo* autoradiography demonstrated 2-fold higher signals in atherosclerotic plaques compared to healthy (no plaque) areas of the aorta (Supplementary Fig. S3D). ^{18}F -FDG SUV_{max} in the ascending aorta showed no significant difference between *ApoE*^{-/-} mice with median of 1.2 (IQR, 1.1-1.5) and C57Bl/6 control animals with median of 1.7 (IQR, 1.4-2.2, $p=0.2$, Fig. 4D and 4E), as also observed by *ex vivo* gamma counting (Fig. 4F). In line with our observations in the myocardial infarction model, in atherosclerotic mice there was a non-significant trend for greater uptake of ^{64}Cu -DOTATATE in $CD11b^+$ cells over $CD11b^-$ cells (2-fold higher when compared to ^{18}F -FDG), and specifically in macrophages (1.5-fold increase when compared to ^{18}F -FDG, $p=0.2$, Fig. 4G and 4H, Supplementary Fig. S3C and Supplementary Table S4).

⁶⁸Ga-DOTATATE's *in vivo* behavior in rabbits

In the next stage of our workflow, we evaluated DOTATATE labeled with the short-lived isotope ⁶⁸Ga in a translational rabbit model of atherosclerosis on a clinical PET/MR scanner. ⁶⁸Ga-DOTATATE pharmacokinetics was assessed in atherosclerotic and non-atherosclerotic (control) New Zealand White (NZW) rabbits (Supplementary Fig. S2A). ⁶⁸Ga-DOTATATE weighted half-life was 53.7 minutes in atherosclerotic rabbits and 21.2 minutes in control animals (Fig. 5A and Supplementary Table S1). In line with findings in mice, the majority of ⁶⁸Ga-DOTATATE was detected in plasma, rather than cells (Supplementary Fig. S4A). At 5 hours post injection, ⁶⁸Ga-DOTATATE median %ID/g in the blood was 1.019 (IQR, 0.902-1.135) in control animals and 1 (IQR, 0.85-2.827) in atherosclerotic rabbits. ⁶⁸Ga-DOTATATE behaved similarly to ⁶⁴Cu-DOTATATE, showing renal clearance and high accumulation in the stomach and other gastrointestinal organs (Fig. 5B and Supplementary Fig. S4B; Supplementary Table S5 and S6). In atherosclerotic rabbits ⁶⁸Ga-DOTATATE median %ID/g in the thoracic and abdominal aorta were, respectively, 0.015 (IQR, 0.011-0.018) and 0.017 (IQR, 0.014-0.022), while, in controls median ⁶⁸Ga-DOTATATE %ID/g was 0.004 (IQR, 0.002-0.006; $p=0.0028$) in the thoracic aorta and 0.006 (IQR, 0.003-0.02; $p=0.1483$) in the abdominal aorta (Fig. 5C and Supplementary Fig. S4B; Supplementary Table S5 and S6).

Translational ⁶⁸Ga-DOTATATE PET/MR imaging of inflammatory atherosclerosis in rabbits

Last, we performed an extensive PET imaging study to assess the quantification of vascular inflammation by ⁶⁸Ga-DOTATATE's and ¹⁸F-FDG in the atherosclerotic rabbit model. Atherosclerotic rabbits at 4 and 7 months after Western diet initiation (athero_{4mo} and athero_{7mo}, respectively) and healthy controls were imaged with both ⁶⁸Ga-DOTATATE and ¹⁸F-FDG on separate days (Supplementary Fig. S2B). Based on pharmacokinetic analysis and dynamic imaging experiments (Supplementary Fig. S4C), we used a circulation time of 120 minutes before PET imaging for ⁶⁸Ga-DOTATATE experiments, whereas ¹⁸F-FDG circulation time was 180 minutes, as previously validated²². Using ⁶⁸Ga-DOTATATE (Fig. 6A), we found a 1.6-fold higher SUV_{max} in atherosclerotic aortas of athero_{4mo} animals as compared to controls, with medians of 0.415 (IQR, 0.338-0.499) and 0.253 (IQR, 0.197-0.285), respectively ($p=0.0002$) (Fig. 6B). However, based on ⁶⁸Ga-DOTATATE PET, we did not detect a further increase in tracer accumulation in rabbits kept on Western Diet for 7 (athero_{7mo}, $p>0.9999$, Fig. 6C). Similar to previous studies²³, we found 1.2-fold higher ¹⁸F-FDG SUV_{max} in the abdominal aorta of athero_{4mo} rabbits, with median 0.446 (IQR, 0.387-0.536), as compared to controls, with median 0.349 (IQR, 0.299-0.423) ($p=0.0159$, Fig. 6D and 6E). ¹⁸F-FDG signal also increased to a median of 0.515 (IQR, 0.409-0.602) over 3 additional months of Western diet (athero_{7mo}, $p=0.0312$, Fig. 6F). Analysis of *ex vivo* near-infrared fluorescence imaging of Cy5.5-labeled HDL in the aorta (a validated marker of macrophage burden²⁴) was in line with ⁶⁸Ga-DOTATATE results: while a significant difference was found in maximum radiant efficiency median values between control 1.67×10^8 (IQR, $1.29 \times 10^8 - 1.94 \times 10^8$) and

atherosclerotic athero_{4mo} animals 4.89×10^9 (IQR, 3.36×10^9 - 6.79×10^9 , $p < 0.0001$), no increase in fluorescent HDL signal was observed when comparing athero_{4mo} and athero_{7mo}, suggesting no increase in macrophage burden over time ($p = 0.5584$, Fig. 6G). A weak, but significant ($r = 0.3522$; $p = 0.0141$), correlation was found between ^{18}F -FDG and ^{68}Ga -DOTATATE aortic SUV_{max} , reflecting the partially overlapping cellular specificity of the two tracers (Supplementary Fig. S4D).

Discussion

Inflammation is pivotal to atherosclerosis development, and a key driver of cardiovascular events such as myocardial infarction^{25,26}. ^{18}F -FDG is the most commonly used PET radiotracer used for the quantification of cardiovascular inflammation *in vivo*. However, several studies have questioned ^{18}F -FDG specificity for inflammatory cells⁹. The tracer's high background uptake in healthy myocardium¹⁰⁻¹², which can only be suppressed using specific fasting protocols in humans or certain anesthesia regimens in animals, is often linked to reproducibility concerns²⁷⁻²⁹. These drawbacks have spurred interest in more inflammation-specific tracers in the cardiovascular arena. Among these, the SSTR2-binding ligand DOTATATE has attracted considerable interest for imaging of the vasculature and heart in humans, as well as in preclinical disease models^{16,17,30}.

In this study, we sought to implement a rigorous framework to thoroughly characterize the *in vivo* behavior of DOTATATE-based radiotracers in comparison with ^{18}F -FDG using mouse models of atherosclerosis and myocardial infarction, as well as a translational rabbit model of atherosclerosis. In mechanistic mouse experiments we labeled DOTATATE with ^{64}Cu . The longer physical half-life of this radioisotope allowed complementing *in vivo* PET imaging with extensive *ex vivo* assays, including flow cytometry, gamma counting, and autoradiography to investigate the tracer pharmacokinetics, timed organ biodistribution, cellular specificity and ability to report on cardiovascular inflammation. In translational PET/MRI rabbit studies we instead used *in vivo* PET imaging with ^{68}Ga -DOTATATE to assess aortic inflammation, in comparison with ^{18}F -FDG.

In mice, thorough pharmacokinetic studies confirmed rapid clearance of ^{64}Cu -DOTATATE from the bloodstream (similar to ^{18}F -FDG, which has a 5.1 minutes half-life)³¹. This feature is important especially for *in vivo* imaging of the vasculature, whose signal can be easily contaminated by the blood pool because of partial volume errors. Timed biodistribution analysis confirmed fast accumulation in the kidneys, bladder and gastrointestinal organs³², and targeting of SSTR2-expressing organs, such as pancreas and adrenal gland.

In light of these findings, we set out to investigate ^{64}Cu -DOTATATE as an inflammation tracer in the context of myocardial infarction and atherosclerosis in mice. For the myocardial infarction model, mice were imaged 3 days after LAD ligation surgery. This timeline was chosen to capture the peak of SSTR2-expressing inflammatory macrophage infiltration in the infarcted myocardium²¹, since SSTR2 is upregulated in inflammatory macrophages/LPS-stimulated macrophages, while expression in other

leukocytes is negligible³³⁻³⁵. A previous preclinical study¹⁹ that investigated ⁶⁸Ga-DOTATATE in mouse models of cardiac ischemia did not show significant DOTATATE accumulation in the infarct. While we also observed low signal in the myocardium, we showed superior infarct detection from the remote myocardium by using ⁶⁴Cu-DOTATATE in comparison with ¹⁸F-FDG, as confirmed by *ex vivo* gamma counting. We used DOTATATE labeled with ⁶⁴Cu, a radioisotope with longer half-life and lower positron range (1 mm) compared to ⁶⁸Ga (4 mm), thereby offering less partial volume effect from the blood stream and intrinsic better signal-to-noise and spatial resolution^{14,16,36}. Our results are also in agreement with the findings of a recent clinical study¹⁸ where focal infarct-related ⁶⁸Ga-DOTATATE signal in patients with MI were well-visualized owing to very low physiological background tracer uptake, and were increased compared to the remote myocardium.

In line with several clinical studies, as well as previous *ex vivo* autoradiography and *in vivo* analysis in *ApoE*^{-/-} mice using ⁶⁸Ga-DOTATATE^{15-17, 30,32,37,38}, we confirmed accumulation of ⁶⁴Cu-DOTATATE in mouse aortic plaques. ⁶⁴Cu-DOTATATE uptake was higher in the aortic arch of atherosclerotic versus control animals, but no differences were detected for ¹⁸F-FDG. While other studies in mice showed higher ¹⁸F-FDG accumulation in atherosclerotic versus control animals^{39,40}, a recent report indicated that the specific anesthesia regimen used, and periaortic fat uptake may significantly affect ¹⁸F-FDG plaque signal⁴¹.

⁶⁴Cu-DOTATATE blood half-life was longer in atherosclerotic mice (and rabbits) compared to controls, a factor that may potentially confound vessel wall readings because of higher blood background signal. We hypothesize that this phenomenon may be attributed to lower renal clearance (due to impaired kidney function) in diseased animals. However, *ex vivo* gamma counting validated the higher aortic tracer accumulation in atherosclerotic versus healthy animals, thereby mitigating these concerns.

Unlike a recently published *in vitro* analysis that employed macrophages differentiated from an immortalized THP-1 cell line⁴², flow cytometry in both mouse models from our study confirmed higher affinity of DOTATATE for myeloid CD11b⁺ cells, with respect to ¹⁸F-FDG, particularly for the macrophage fraction. This discrepancy might be attributed to methodological differences between the two studies, such as our studies being conducted *in vivo*, in mouse models, as opposed to *in vitro*, in cells derived from human blood, as well as the different cell isolation protocols. Our results are in line with a recent clinical study that confirmed high expression of SSTR2 in human M1 inflammatory macrophages, in comparison with other myeloid and immune cells. However, glucose transporters 1 and 3 (GLUT1 and GLUT3) were found to be highly expressed by all immune cells, corroborating the lower cellular specificity of ¹⁸F-FDG¹⁷.

In addition to the extensive mechanistic mouse work, we evaluated ⁶⁸Ga-DOTATATE in a rabbit model of atherosclerosis. *Ex vivo* quantification of aortic HDL accumulation (a marker of macrophage burden) by near-infrared fluorescence imaging was in line with the *in vivo* ⁶⁸Ga-DOTATATE readout, indicating no

increased macrophage burden during atherosclerosis progression. These findings strengthen the notion that the two tracers report on inter-related but intrinsically different processes.

In this study we thoroughly characterized the PET tracer DOTATATE in comparison with ^{18}F -FDG in small animal models of atherosclerosis and myocardial infarction using a combination of *in vivo* PET imaging and extensive *ex vivo* readouts. Our results support the use of DOTATATE-based radiotracers for a more targeted assessment of cardiovascular inflammation, as alternative and complement to the widely used metabolic tracer ^{18}F -FDG. Furthermore, our study establishes a functional workflow for the in-depth comparison of different PET radiotracers in the cardiovascular field of research.

Methods

Radiolabeling of DOTA-(Tyr³)-Octreotate with Copper-64 ^{64}Cu

DOTA-(Tyr³)-Octreotate (DOTATATE) acetate salt was purchased from Bachem (Bubendorf, Switzerland). ^{64}Cu was produced using a CS15 cyclotron located at Washington University by the $^{64}\text{Ni}[\text{p,n}]^{64}\text{Cu}$ nuclear reaction. Activity measurements were made using a Capintec CRC-15R Dose Calibrator (Capintec, Florham Park, NJ). ^{64}Cu was chelated to DOTATATE by adjusting the pH of a ^{64}Cu solution to 5, using a buffer containing 0.1 M NH_4OAc . Subsequently, 20 μg of DOTATATE were added to the solution and the reaction mixture was heated at 80 °C for approximately 45 minutes. The labeling reaction yielded ^{64}Cu -DOTATATE with a radiochemical purity of >98%, as determined by RadioHPLC.

High-performance liquid chromatography (HPLC) and radio-HPLC.

High-performance liquid chromatography (HPLC) was performed on a Shimadzu (Kyoto, Japan) HPLC system equipped with two LC-10AT pumps and an SPD-M10AVP photodiode array detector. Radio-HPLC was performed using a Lablogic (Tampa, FL) Scan-RAM Radio-TLC/HPLC detector. Reverse phase chromatography was performed using a Waters Atlantis T3 column, 100, 5 μm , 4.6 mm x 250 mm (Waters, Milford, MA) with an acetonitrile to water gradient from 5-95% acetonitrile over 20 minutes at a flow rate of 1.0 mL min^{-1} .

Animal experiments

All animal experiments were performed in accordance with protocols approved by the Institutional Animal Care and Use Committee at the Icahn School of Medicine at Mount Sinai and followed National Institutes of Health guidelines for animal welfare. This study is reported in accordance with ARRIVE guidelines.

Mouse model

Animals were housed under a constant room temperature at 25 ± 2 °C and $50 \pm 5\%$ humidity with a 12-hour daylight period and 12-hour darkness period, with free access to water. For the mouse atherosclerosis model, 8-weeks old female *ApoE*^{-/-} mice (N=51) were purchased from Jackson

Laboratories (Bar Harbor, ME) and, after a 48 hours acclimatization period, were fed a Western Diet (42% Kcal from fat TD88137, Envigo, Huntingdon, UK) for 12 weeks. Age-matched female C57Bl/6 controls (N=67) were kept on regular chow diet. The myocardial infarction group consisted 16-20 weeks old female C57Bl/6 mice (N=18) purchased from Jackson Laboratories and subjected to ligation of the left anterior descending artery, as previously described⁴³.

Rabbit model

For the rabbit atherosclerosis model, 3-month old male New Zealand White (NZW) rabbits (N=39) were purchased from Charles River Laboratories (Wilmington, MA) and placed on Western diet (initial 8 weeks on regular chow enriched with 0.3% cholesterol and 4.7% coconut oil, and the remaining time period on 0.15% enriched cholesterol diet from Research diets, Inc. Brunswick, NJ). Randomly assigned control rabbits (N=12) were kept on chow diet. In order to induce atherosclerotic lesions, rabbits were subjected to two endothelial denudations of the aorta through the right and left femoral artery at 2 and 6 weeks after diet initiation, respectively, as described previously⁴⁴. Rabbits with atherosclerosis (N=36) were imaged 4 months after diet initiation and euthanized to establish disease characteristics. The remaining atherosclerotic rabbits were fed a Western diet for an additional 3 months (N=9) to advance atherosclerosis. At the end of the 3-month period, these rabbits were imaged and euthanized.

Myocardial infarction surgery in mice

Myocardial infarction in mice was induced by permanent ligation of the left anterior descending (LAD) coronary artery of female C57Bl/6 mice (N=18). Briefly, animals were anesthetized with xylazine (10 mg/Kg) and ketamine (100 mg/Kg) and intubated using an endotracheal intubation kit from Braintree Scientific (Braintree, MA). Left-sided thoracotomy and pericardial incision were performed. A 7-0 Silk suture was used to occlude the LAD. Incisions were closed with a 5-0 Silk suture. Infarcted animals were treated with 0.1 mg/Kg of buprenorphine every 12 hours and used 3 days after the surgery.

⁶⁴Cu-DOTATATE biodistribution, pharmacokinetics and blood separation analysis in mice

For biodistribution, pharmacokinetics and blood separation analysis in mice we used ⁶⁴Cu-labeled DOTATATE due to this isotope's longer physical half-life compared to ⁶⁸Ga (12.7 vs 1.1 hours), which allowed us to perform extensive *ex vivo* validation assays. Wild-type and atherosclerotic animals were injected with approximately 1.85 MBq of ⁶⁴Cu-DOTATATE and euthanized at either 1, 5, 15, 30, 60 or 120 minutes after injection (Supplementary Fig. S1A) to evaluate the tracer's biodistribution. Mice were perfused with 20 mL of phosphate-buffered saline (PBS) and tissues of interest (blood, heart, aorta, bone marrow, spleen, liver, stomach, bladder, kidneys, intestines, lungs, adrenal gland, muscles and pancreas) were harvested. Tissues were blotted for gamma counting on a Wizard2 2480 automatic gamma counter (Perkin Elmer, Waltham, MA). Values were corrected for decay and normalized to tissue weight to express radioactivity concentration as percentage injected dose per gram (%ID/g). Blood half-life was calculated by measuring blood radioactivity over time for 120 minutes and data were fitted using a two-phase decay

non-linear regression using GraphPad Prism v8.4.3 (Supplementary Table S1). To investigate the tracer's distribution within different blood compartments, after gamma counting, 100 μ L of blood were spun down at 2000g for 15 minutes at 4°C. Plasma (supernatant) and cells (pellet) were gamma counted and expressed as percentage of total activity. The remainder of the blood was separated using Lymphoprep density gradient medium (Nycomed Pharma, Zurich, Switzerland) following manufacturer's instructions. Percentage of activity in mononuclear and polynuclear cells was calculated.

***In vivo* PET/CT imaging in mice**

For the PET/CT experiments, mice were fasted for 12 hours before radiotracer injection and anesthetized with xylazine (10 mg/kg) and ketamine (100 mg/kg) through intraperitoneal injection prior to radiotracer administration. Subsequently they were injected via the lateral tail vein with approximately 22.2 MBq of ^{18}F -FDG or 5.55 MBq of ^{64}Cu -DOTATATE. Tracers were allowed to circulate for 60 minutes. Immediately before imaging, mice were placed under 1% isoflurane (BaxterHealthcare, Deerfield, IL), and subsequently imaged on a Mediso nanoScan PET/CT scanner (Mediso, Budapest, Hungary). High resolution CT scan was acquired at 50 kVp and 300 ms exposure per projection. eXIA160 (Binitio, Ontario, Canada) was used as a contrast agent to improve imaging of the vasculature by intravenous administration of 100 μ l per mouse 5 minutes prior to CT acquisition⁴⁵. PET acquisition time was 40 minutes. Reconstruction was performed using TeraTomo 3D reconstruction engine, for 8 iterations and 6 subsets per iteration for both tracers. The voxel size was isotropic at 0.3 mm. Immediately after the PET/CT scan, animals were euthanized for *ex vivo* assays.

Flow cytometry

After PET imaging, mouse hearts and aortas were harvested and collected in PBS-filled tubes. Aortas were minced and digested with an enzymatic digestion solution containing liberase TH (4 U/ml) (Roche, Basel, Switzerland), DNase I (40 U/ml) and hyaluronidase (60 U/ml) in PBS. Heart tissue was minced and digested using an enzymatic digestion solution containing DNase I (60 U/ml), collagenase type I (450 U/ml), collagenase type XI (125 U/ml) and hyaluronidase (60 U/ml) in PBS. Samples were treated with the respective enzymatic solution for 60 minutes at 37 °C. All enzymes were purchased from Sigma-Aldrich (St. Louis, MO). Samples were then passed through a 70 μ m filter, washed and prepared for antibody staining and flow sorting. Cellular fragments and debris were gated out of the analysis by utilizing forward and side angle light scatter signal. Macrophages were identified as Ly6G⁻ (Clone 1A8, PE/Cy7), CD11b⁺ (Clone M1/70, PE), CD11c⁻ (Clone N418, PerCP/Cy5.5) and F4/80⁺ (Alexa Fluor[®] 647, Clone BM8) from Biolegend (San Diego, CA). The remaining CD11b⁺ cells were identified as Ly6G^{lo}, CD11b^{hi}, CD11c^{hi}. Data were acquired on a FACS Aria flow sorter (BD Biosciences, East Rutherford, NJ) and analyzed using FlowJo v10.0.7 (Tree Star, Ashland, OR). Sorted cells were gamma counted and activity per cell values were calculated.

Autoradiography

Tissues (heart and aorta) were placed in a film cassette against a phosphorimaging plate (BASMS-2325, Fujifilm) at -20°C to determine the regional radioactivity distribution. The plates were read at a pixel resolution of $25\ \mu\text{m}$ with a Typhoon 7000IP plate reader (GE Healthcare, Pittsburgh, PA). Images were analyzed using ImageJ software v1.52 (Madison, WI).

^{68}Ga -DOTATATE biodistribution, pharmacokinetics and blood separation analysis in rabbits

Adopting a translational approach, the rabbit studies were performed with the ^{68}Ga -labeled tracer, which is already being used in the clinic. ^{68}Ga -DOTATATE was purchased from Advanced Accelerator Applications (AAA, Millburn, NJ, USA). To determine its pharmacokinetics, three atherosclerotic rabbits and two healthy controls were injected with approximately 190 MBq of ^{68}Ga -DOTATATE. Arterial blood was sampled at 1, 5, 10, 15, 20, 30, 60, 120, 180, 240 and 300 minutes after injection through the ear vein. Samples were weighed and gamma counted. Blood half-life data were fitted using a two-phase decay non-linear regression using GraphPad Prism v8.4.3 (Supplementary Table S1). To investigate the tracer blood distribution, blood samples were centrifuged at 2000g for 15 minutes at 4°C to determine the radioactivity concentration in the plasma and cellular fractions. To analyze ^{68}Ga -DOTATATE biodistribution, all rabbits were euthanized after the last imaging time-point using an injection of pentobarbital 100 mg/kg and exsanguination of the portal vein. Rabbits were extensively perfused with 1000 mL of saline. Following, tissues (blood, heart, aorta, liver, kidney, skeletal muscle, small and large intestine, fat, stomach, pancreas and bladder) were harvested, weighed and gamma counted.

***In vivo* PET/MR imaging in rabbits**

In vivo imaging in rabbits was performed on a 3 Tesla Biograph mMR (Siemens, Erlangen, Germany) Positron Emission Tomography/Magnetic Resonance Imaging (PET/MRI) clinical scanner. To establish the optimal imaging time-point for ^{68}Ga -DOTATATE aortic imaging in this animal model, 5 rabbits underwent dynamic PET imaging for 3 hours immediately after injection of approximately 190 MBq of the tracer. Rabbits were injected intravenously via the ear vein with approximately 190 MBq of either ^{18}F -FDG or ^{68}Ga -DOTATATE. Rabbits undergoing ^{18}F -FDG scans were fasted for 3-4 hours before injection to avoid tracer uptake in the bowels, as previously validated ⁴⁶. After injection, ^{18}F -FDG was allowed to circulate for 3 hours, as per previously described ²², while, based on results of dynamic analyses, ^{68}Ga -DOTATATE was left to circulate for 2 hours. At the end of the circulation time, rabbits were anesthetized with ketamine (20 mg/kg) and xylazine (5mg/kg) i.m. Animals were then placed in supine position under 1.5% isoflurane inhalation on the PET/MR scanner. After scout scans, PET imaging was initiated for 30 minutes for ^{18}F -FDG and 60 minutes for ^{68}Ga -DOTATATE. 3D non contrast enhanced time-of-flight (TOF) images were acquired to visualize the abdominal aorta and renal arteries, with the following imaging parameters: repetition time (TR), 23 ms; echo time (TE), 2.8 ms; flip angle, 20 degrees; spatial resolution, $0.35\ \text{mm}^2$ (interpolated); slice thickness, 1 mm. PET images were reconstructed offline. Attenuation correction of PET images was performed by using a vendor built-in Dixon MR- based attenuation map (MR-AC) with 2 (soft tissue, air). Images were reconstructed using a 3D ordinary Poisson

ordered subsets expectation maximization (OP-OSEM) algorithm with point-spread-function (PSF) resolution modeling, using 3 iterations and 21 subsets and filtered with a 4 mm Gaussian filter. Animals were then euthanized, perfused and aortas were collected for gamma counting.

⁶⁴Cu-DOTATATE, ⁶⁸Ga-DOTATATE and ¹⁸F-FDG PET image analysis

Using OsiriX v5.6 software (OsiriX Foundation, Geneva, Switzerland), regions of interest (ROIs) were drawn to determine organ radioactivity concentration. In mice, for healthy and infarcted myocardium, ROIs were traced manually in the apex of the heart in the axial view. For remote myocardium, analysis was performed in myocardium 180° from the infarcted zone. In the mice aorta, sequential ROIs were drawn in the ascending aorta from the root up to the brachiocephalic branch. Voxel counts were converted to maximum standardized uptake values (SUV_{max}). In rabbits, PET images were fused with time-of-flight bright blood MRI angiography and ROIs were manually drawn on the infrarenal abdominal aorta in TOF images. The slice-by-slice maximum standard uptake values (SUV_{max}) were averaged across the whole aorta. To ensure blinding, investigator involved in the imaging analysis was not aware of the group distribution in the imaging slices.

Near infrared fluorescence imaging in of rabbit aortas

Ex vivo near infrared fluorescence imaging of rabbit aortas was performed on a Xenogen IVIS Spectrum Preclinical Imaging System (Perkin Elmer, Waltham, MA). Approximately 24 hours before euthanasia, animals were injected with Cy5.5-labeled high-density lipoprotein (HDL), which was used to determine macrophage burden. Fluorescence images were obtained with the following excitation and emission band-pass filter parameters: λ excitation = 640 ± 18 nm, λ emission = 720 ± 10 nm. Images were subsequently analyzed by dividing the infrarenal abdominal aorta into 8 ROIs of the same size. Max radiant efficiency [$(p/s/cm^2/sr)/(\mu W/cm^2)$] for each ROI were recorded as a measure Cy5.5-HDL deposition in the aorta.

Statistics

All results are presented as mean \pm standard error of the mean (SEM) or median and interquartile range (IQR). After running appropriate tests for normality, non-parametric statistical tests were deemed appropriate. Unpaired data were analyzed with non-parametric Mann-Whitney tests. Analysis of longitudinal imaging studies were performed using Wilcoxon matched-pairs signed rank tests. Correlation of ⁶⁸Ga-DOTATATE maximum standardized uptake value (SUV_{max}) and ¹⁸F-FDG SUV_{max} was calculated by computing a nonparametric Spearman coefficient. For all tests, $\alpha < 0.05$ represents statistical significance. Levels of significance were indicated as follows: * $p < 0.05$, ** $p < 0.01$, *** $p < 0.001$, **** $p < 0.0001$.

Declarations

Data availability

The datasets generated during and/or analysed during the current study are available from the corresponding author on reasonable request.

Author contributions statement

Specific author contributions are as follows:

Y.C.T. and A.A.G.: design and execution of experiments and analyses, manuscript writing. S.N., K.S., M.M.T.v.L., S.J., F.O., L.A., A.M.S., E.L.F., A.M., N.S., J.M., M.L.S., C.M., G.S.: execution of experiments. T.R., J.M.T., J.H.F.R., C.G., J.O., C.P.M., A.K., W.J.M.M., Z.A.F.: design and supervision of experiments and analysis, manuscript writing and revisions. C.C.: study design, experiment and analysis design, manuscript concept and writing, data integrity.

Additional information

Competing interests

Andreas Kjaer is an inventor on a patent/holds IPR regarding the use of ^{64}Cu -DOTATATE in neuroendocrine tumor patients. The other authors report no Relationship with Industry and Other Entities. No other potential conflicts of interest relevant to this article exist.

Sources of funding:

AAG was supported by The Lundbeck Foundation R251-2017-870. FO was supported by an Institutional Research Training Grant T32CA078207. AM was supported by Deutsche Forschungsgemeinschaft MA7059/1. TR was supported by MSK Cancer Center P30 P30 CA008748. JMT was supported by the Wellcome Trust (211100/Z/18/Z). JHFR is part-supported by the NIHR Cambridge Biomedical Research Centre, the British Heart Foundation, Higher Education Funding Council for England, the Engineering and Physical Sciences Research Council and the Wellcome Trust. CG was supported by NIH-NHLBI R01 HL153712-01, NIH-NCATS UH3TR002067, American Heart Association 20SFRN35210252 and Chan Zuckerberg Initiative NFL-2020-218415. ZAF was supported by NIH/NHLBI R01 HL135878.

References

1. Virani, S. S. *et al.* Heart disease and stroke statistics—2020 update: A report from the American Heart Association. *Circulation* (2020). doi:10.1161/CIR.0000000000000757.
2. Dutta, P. *et al.* Myocardial infarction accelerates atherosclerosis. *Nature* **487**, 325–329 (2012).
3. Tomas, L. *et al.* Altered metabolism distinguishes high-risk from stable carotid atherosclerotic plaques. *Eur. Heart J.* **39**, 2301–2310 (2018).
4. Fernandez, D. M. *et al.* Single-cell immune landscape of human atherosclerotic plaques. *Nat. Med.* **25**, 1576–1588 (2019).

5. Ridker, P. M. *et al.* Antiinflammatory therapy with canakinumab for atherosclerotic disease. *N. Engl. J. Med.* **377**, 1119–1131 (2017).
6. Tardif, J. *et al.* Efficacy and Safety of Low-Dose Colchicine after Myocardial Infarction To cite this version: HAL Id: hal-02368804. (2020).
7. Kircher, M. & Lapa, C. Novel Noninvasive Nuclear Medicine Imaging Techniques for Cardiac Inflammation. *Curr. Cardiovasc. Imaging Rep.* **10**, (2017).
8. Maschauer, S., Prante, O., Hoffmann, M., Deichen, J. T. & Kuwert, T. Characterization of 18F-FDG uptake in human endothelial cells in vitro. *J. Nucl. Med.* **45**, 455–460 (2004).
9. Al-Mashhadi, R. H. *et al.* 18Fluorodeoxyglucose Accumulation in Arterial Tissues Determined by PET Signal Analysis. *J. Am. Coll. Cardiol.* **74**, 1220–1232 (2019).
10. Manabe, O. *et al.* Radiopharmaceutical tracers for cardiac imaging. *J. Nucl. Cardiol.* **25**, 1204–1236 (2018).
11. Inglese, E. *et al.* Spatial and temporal heterogeneity of regional myocardial uptake in patients without heart disease under fasting conditions on repeated whole-body 18F-FDG PET/CT. *J. Nucl. Med.* **48**, 1662–1669 (2007).
12. Gropler, R. J. *et al.* Nonuniformity in myocardial accumulation of fluorine-18-fluorodeoxyglucose in normal fasted humans. *J. Nucl. Med.* **31**, 1749–1756 (1990).
13. Gipharma S.r.l. NETSPOT (kit for the preparation of gallium Ga 68 dotatate injection). 1–13 (2016).
14. Johnbeck, C. B. *et al.* Head-to-Head Comparison of 64Cu-DOTATATE and 68Ga-DOTATOC PET/CT: A prospective study of 59 patients with neuroendocrine tumors. *J. Nucl. Med.* **58**, 451–457 (2017).
15. Li, X. *et al.* Specific somatostatin receptor II expression in arterial plaque: 68Ga-DOTATATE autoradiographic, immunohistochemical and flow cytometric studies in apoE-deficient mice. *Atherosclerosis* **230**, 33–39 (2013).
16. Malmberg, C. *et al.* 64Cu-DOTATATE for noninvasive assessment of atherosclerosis in large arteries and its correlation with risk factors: Head-to-head comparison with 68Ga-DOTATOC in 60 patients. *J. Nucl. Med.* **56**, 1895–1900 (2015).
17. Tarkin, J. M. *et al.* Detection of Atherosclerotic Inflammation by 68Ga-DOTATATE PET Compared to [18F]FDG PET Imaging. *J. Am. Coll. Cardiol.* **69**, 1774–1791 (2017).
18. Tarkin, J. M. *et al.* 68Ga-DOTATATE PET Identifies Residual Myocardial Inflammation and Bone Marrow Activation After Myocardial Infarction. *J. Am. Coll. Cardiol.* **73**, 2489–2491 (2019).
19. Thackeray, J. T. *et al.* Targeting post-infarct inflammation by PET imaging: comparison of 68Ga-citrate and 68Ga-DOTATATE with 18F-FDG in a mouse model. *Eur. J. Nucl. Med. Mol. Imaging* **42**, 317–327 (2015).
20. Lee, W. W. *et al.* PET/MRI of inflammation in myocardial infarction. *J. Am. Coll. Cardiol.* (2012) doi:10.1016/j.jacc.2011.08.066.
21. Thackeray, J. T. & Bengel, F. M. Molecular Imaging of Myocardial Inflammation With Positron Emission Tomography Post-Ischemia: A Determinant of Subsequent Remodeling or Recovery. *JACC*

- Cardiovasc. Imaging* **11**, 1340–1355 (2018).
22. Tawakol, A. *et al.* Noninvasive in vivo measurement of vascular inflammation with F-18 fluorodeoxyglucose positron emission tomography. *J. Nucl. Cardiol.* **12**, 294–301 (2005).
 23. Zhao, Q. ming *et al.* Detection of Vulnerable Atherosclerotic Plaque and Prediction of Thrombosis Events in a Rabbit Model Using 18F-FDG -PET/CT. *PLoS One* **8**, 1–9 (2013).
 24. Pelosi, G. *et al.* Inflammation blood and tissue factors of plaque growth in an experimental model evidenced by a systems approach. *Front. Genet.* **5**, 1–6 (2014).
 25. Willerson, J. T. & Ridker, P. M. Inflammation as a cardiovascular risk factor. *Circulation* **109**, 2–10 (2004).
 26. Viola, J. & Soehnlein, O. Atherosclerosis - A matter of unresolved inflammation. *Semin. Immunol.* **27**, 184–193 (2015).
 27. Kumar, P., Patel, C. D., Singla, S. & Malhotra, A. Effect of duration of fasting and diet on the myocardial uptake of F-18-2-fluoro-2-deoxyglucose (F-18 FDG) at rest. *Indian J. Nucl. Med.* **29**, 140–145 (2014).
 28. Huet, P., Burg, S., Le Guludec, D., Hyafil, F. & Buvat, I. Variability and uncertainty of 18F-FDG PET imaging protocols for assessing inflammation in atherosclerosis: Suggestions for improvement. *J. Nucl. Med.* **56**, 552–559 (2015).
 29. Bhambhvani, P. Challenges of cardiac inflammation imaging with F-18 FDG positron emission tomography. *J. Nucl. Cardiol.* **24**, 100–102 (2017).
 30. Pedersen, S. F. *et al.* 64Cu-DOTATATE PET/MRI for detection of activated macrophages in carotid atherosclerotic plaques: Studies in patients undergoing endarterectomy. *Arterioscler. Thromb. Vasc. Biol.* **35**, 1696–1703 (2015).
 31. Liu, R. S. *et al.* Biodistribution, pharmacokinetics and PET Imaging of [18F]FMISO, [18F]FDG and [18F]FAc in a sarcoma- and inflammation-bearing mouse model. *Nucl. Med. Biol.* **36**, 305–312 (2009).
 32. Rinne, P. *et al.* Comparison of Somatostatin Receptor 2-Targeting PET Tracers in the Detection of Mouse Atherosclerotic Plaques. *Mol. Imaging Biol.* **18**, 99–108 (2016).
 33. Tarkin, J. M., Joshi, F. R. & Rudd, J. H. F. PET imaging of inflammation in atherosclerosis. *Nat. Rev. Cardiol.* **11**, 443–457 (2014).
 34. Perez, J. *et al.* Somatostatin binds to murine macrophages through two distinct subsets of receptors. *J. Neuroimmunol.* **138**, 38–44 (2003).
 35. Dalm, V. A. S. H. *et al.* Expression of somatostatin, cortistatin, and somatostatin receptors in human monocytes, macrophages, and dendritic cells. *Am. J. Physiol. - Endocrinol. Metab.* **285**, 344–353 (2003).
 36. Fani, M., André, J. P. & Maecke, H. R. 68Ga-PET: A powerful generator-based alternative to cyclotron-based PET radiopharmaceuticals. *Contrast Media Mol. Imaging* **3**, 53–63 (2008).

37. Mojtahedi, A. *et al.* Assessment of vulnerable atherosclerotic and fibrotic plaques in coronary arteries using (68)Ga-DOTATATE PET/CT. *Am. J. Nucl. Med. Mol. Imaging* **5**, 65–71 (2015).
38. Rominger, A. *et al.* In vivo imaging of macrophage activity in the coronary arteries using 68Ga-DOTATATE PET/CT: Correlation with coronary calcium burden and risk factors. *J. Nucl. Med.* **51**, 193–197 (2010).
39. Hag, A. M. F. *et al.* 18F-FDG PET Imaging of Murine Atherosclerosis: Association with Gene Expression of Key Molecular Markers. *PLoS One* **7**, (2012).
40. Hellberg, S. *et al.* Effects of atorvastatin and diet interventions on atherosclerotic plaque inflammation and [18F]FDG uptake in Ldlr^{-/-}-Apob100/100 mice. *Atherosclerosis* **263**, 369–376 (2017).
41. Toczek, J. *et al.* Periaortic brown adipose tissue as a major determinant of [18F]-fluorodeoxyglucose vascular uptake in atherosclerosis-prone, ApoE^{-/-} mice. *PLoS One* **9**, 1–9 (2014).
42. Borchert, T. *et al.* Dissecting the target leukocyte subpopulations of clinically relevant inflammation radiopharmaceuticals. *J. Nucl. Cardiol.* (2019) doi:10.1007/s12350-019-01929-z.
43. Tarnavski, O. *et al.* Mouse cardiac surgery: Comprehensive techniques for the generation of mouse models of human diseases and their application for genomic studies. *Physiol. Genomics* **16**, 349–360 (2004).
44. Binderup, T. *et al.* Imaging-assisted nanoimmunotherapy for atherosclerosis in multiple species. *Sci. Transl. Med.* **11**, (2019).
45. Xing, R. *et al.* Contrast-enhanced micro-CT imaging in murine carotid arteries: A new protocol for computing wall shear stress. *Biomed. Eng. Online* **15**, 621–636 (2016).
46. Lederman, R. J. *et al.* Detection of atherosclerosis using a novel positron-sensitive probe and 18-fluorodeoxyglucose (FDG). *Nucl. Med. Commun.* **22**, 747–753 (2001).

Figures

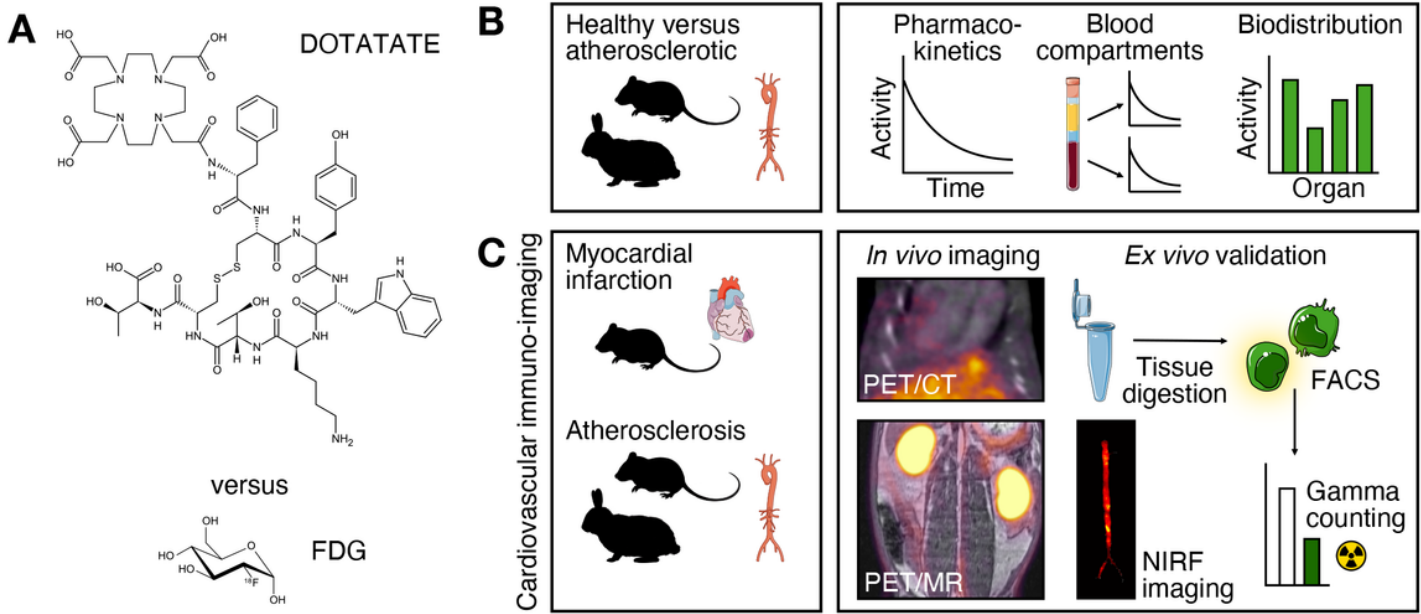


Figure 1

Study design. A) The chemical structure of DOTATATE (top) consists of tyrosine3-octreotate, a somatostatin receptor ligand, covalently bound to the chelator DOTA. 18F-FDG (bottom) is a glucose analog with a fluorine-18 replacing the C-2 hydroxyl group. B) Pharmacokinetics and biodistribution overview. DOTATATE biodistribution and pharmacokinetics were obtained by ex vivo gamma counting of blood and organs. C) In mice, comparison of 64Cu-DOTATATE and 18F-FDG in models of myocardial infarction and atherosclerosis was performed by in vivo PET/CT, while tracers' cellular uptake was determined by flow cytometry in heart and aortic tissue. Translational rabbit study overview. Animals were imaged by in vivo PET/MRI using 68Ga-DOTATATE and 18F-FDG. Results were validated by ex vivo gamma counting and near-infrared fluorescence imaging.

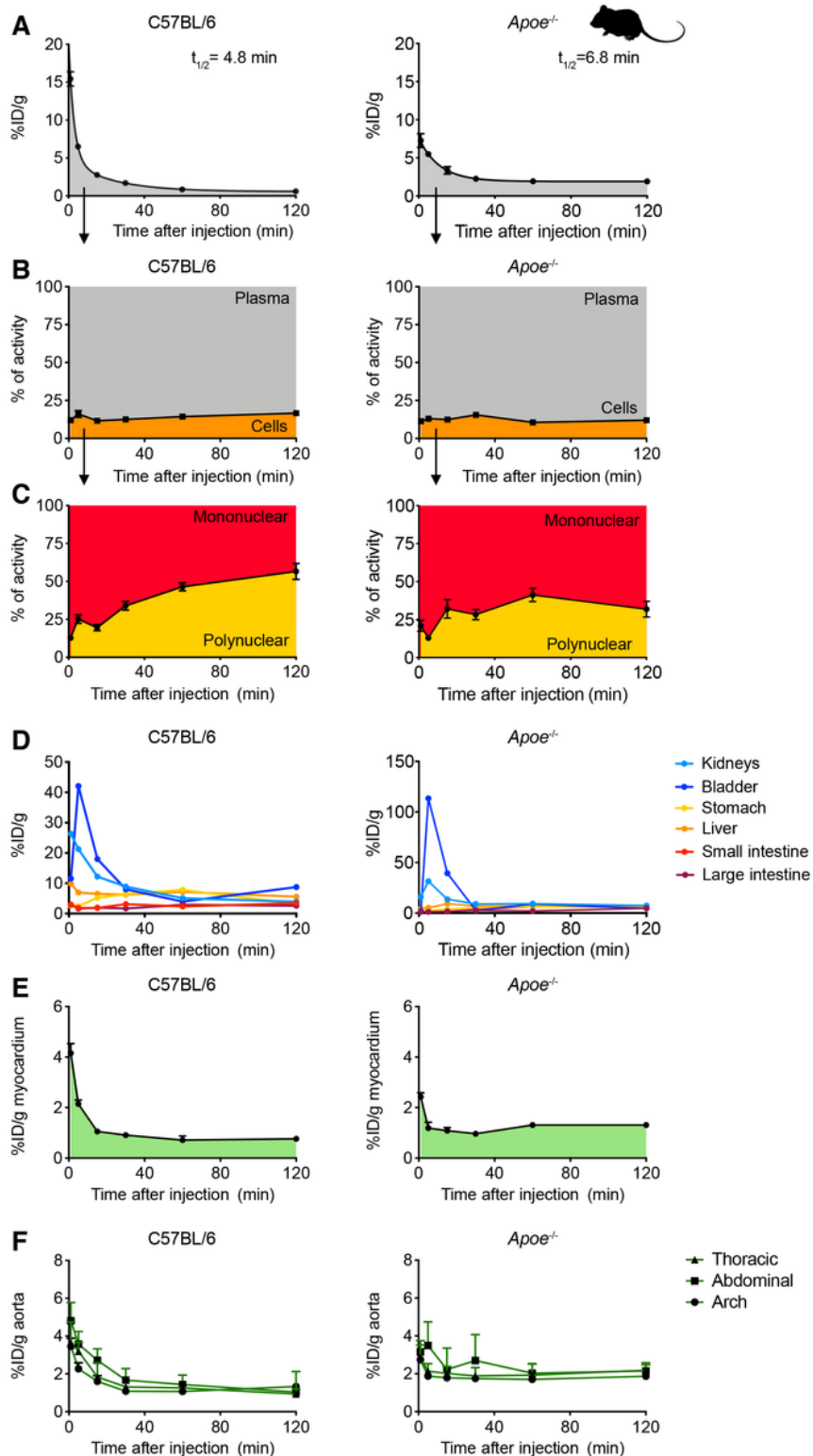


Figure 2

⁶⁴Cu-DOTATATE pharmacokinetics and biodistribution in mice. A) Blood time-activity curve for intravenously infused ⁶⁴Cu-DOTATATE in C57BL/6 (left) and *Apoe*^{-/-} (right) mice. Data are presented as mean ± standard error of the mean. B) ⁶⁴Cu-DOTATATE radioactivity distribution in blood fractions as measured by gamma counting. Graphs show the percentage of activity associated with cells or plasma. Data are presented as mean ± standard error of the mean. C) Percentage of activity associated with

blood mononuclear or polynuclear cells. Data are presented as mean \pm standard error of the mean. D) Time-activity curves for ^{64}Cu -DOTATATE in clearance organs. E) Gamma counting of ^{64}Cu -DOTATATE activity in the myocardium over time. Data are presented as median (interquartile range). F) Time-activity curves for ^{64}Cu -DOTATATE in the arch, thoracic and abdominal aorta. Data are presented as median (interquartile range). ID: injected dose; $t_{1/2}$: half-life. N=5-7 per time-point.

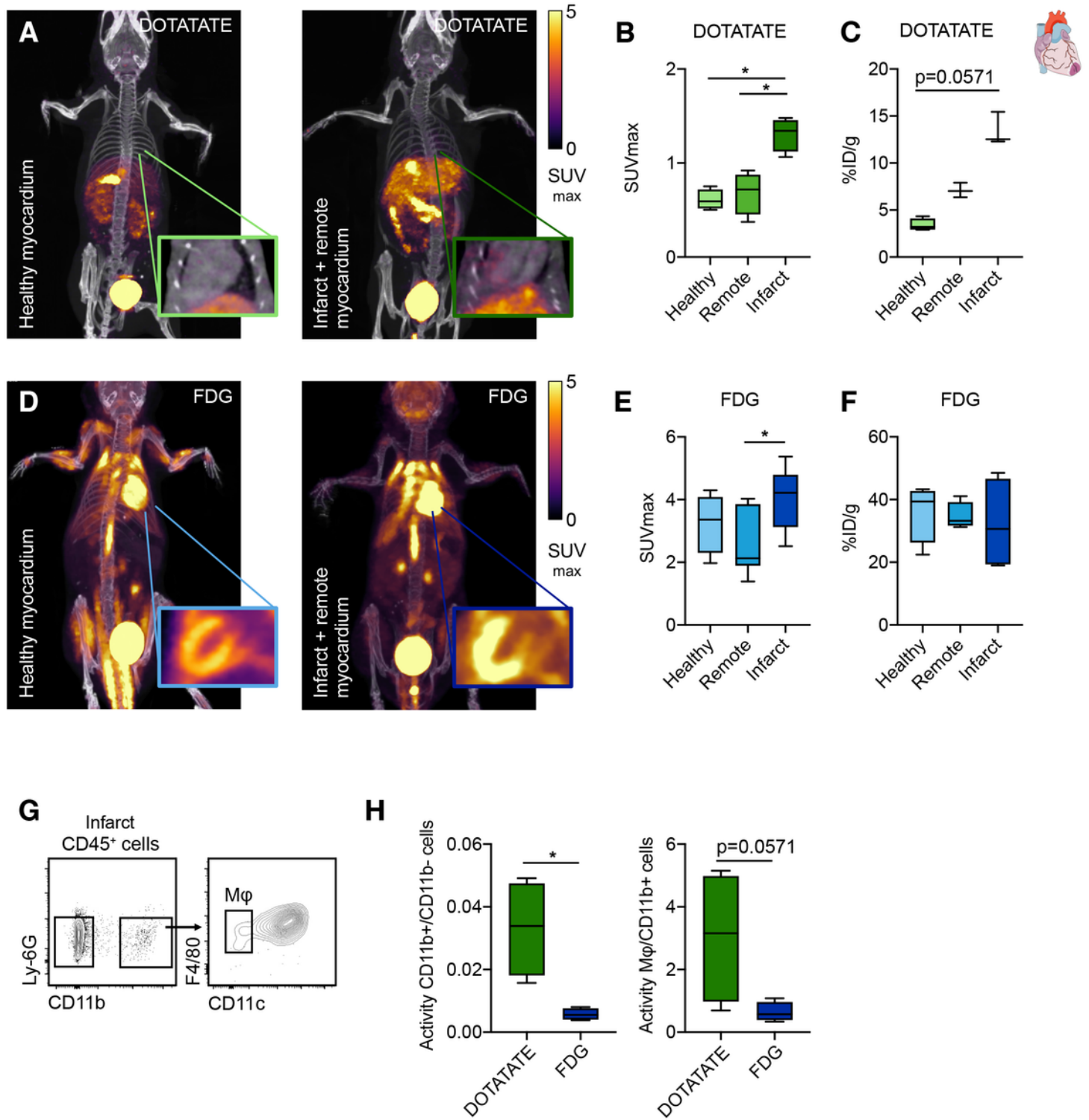


Figure 3

⁶⁴Cu-DOTATATE PET imaging of murine myocardial infarction. A) Representative fused ⁶⁴Cu-DOTATATE PET/CT 3D-rendered images of healthy (left) and LAD-ligated (right) animals, including a magnified heart showing myocardial uptake. B) ⁶⁴Cu-DOTATATE SUVmax (in vivo) and C) %ID/g (ex vivo) in the heart of C57Bl/6 healthy animals (myocardium) and LAD-ligated mice (remote and infarct). D) Representative fused ¹⁸F-FDG PET/CT 3D-rendered images of healthy (left) and LAD-ligated (right) animals, including a magnified heart showing myocardium uptake. E) ¹⁸F-FDG SUVmax (in vivo) and F) %ID/g (ex vivo) in the heart of C57Bl/6 healthy animals (myocardium) and LAD-ligated mice (remote and infarct). G) Representative flow cytometry plots identifying CD11b⁻, CD11b⁺ and macrophage cell populations in the myocardium. H) Quantification of activity per cell in the infarcted myocardium. Data are expressed as ratio of CD11b⁺/CD11b⁻ (left) and Mφ/CD11b⁺ cell activity (right). DOTATATE: ⁶⁴Cu-DOTATATE; FDG: ¹⁸F-FDG; infarct: infarcted region of the myocardium; ID: injected dose; Mφ: macrophages; Myocardium: healthy C57Bl/6 myocardium; remote: remote myocardium (non-infarcted); SUVmax: maximum standardized uptake value. CD11b⁺ cells represent CD11b⁺CD11chi, excluding macrophage population. *p<0.05. N=4-6 animals per group. Data are presented as median (interquartile range).

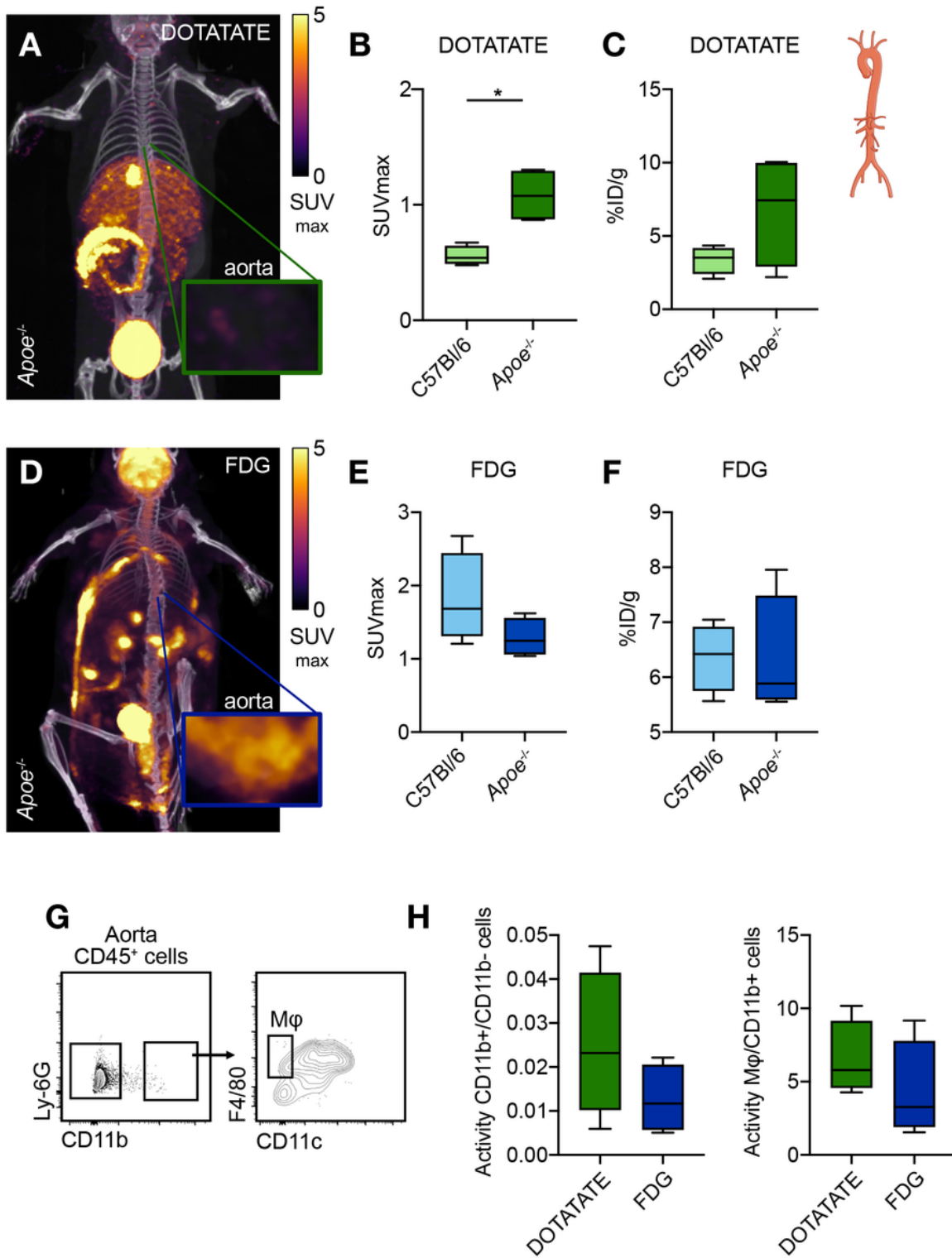


Figure 4

⁶⁴Cu-DOTATATE PET imaging of murine atherosclerosis. A) Representative fused PET/CT 3D-rendered image of ⁶⁴Cu-DOTATATE-infused Apoe^{-/-} mice after 12 weeks on Western Diet (WD). Magnification shows aortic root. B) In vivo ⁶⁴Cu-DOTATATE SUVmax of the ascending aorta. C) Ex vivo %ID/g of the whole aorta. D) Representative fused PET/CT 3D-rendered image of ¹⁸F-FDG-infused Apoe^{-/-} mice. Magnification shows aortic root. E) ¹⁸F-FDG SUVmax of ascending aorta. F) %ID/g of the whole aorta. G)

Representative flow cytometry plots identifying CD11b+ and macrophage cell populations in the aorta. H) Quantification of activity per cell in the aorta. Data are expressed as ratio of CD11b+/CD11b- (left) and M ϕ /CD11b+ cell activity (right). DOTATATE: ⁶⁴Cu-DOTATATE; FDG: ¹⁸F-FDG; ID: injected dose; M ϕ : macrophages; SUVmax: maximum standardized uptake value. CD11b+ cells represent CD11b+CD11chi, excluding macrophage population. *p<0.05. N=4 animals per group. Data are presented as median (interquartile range).

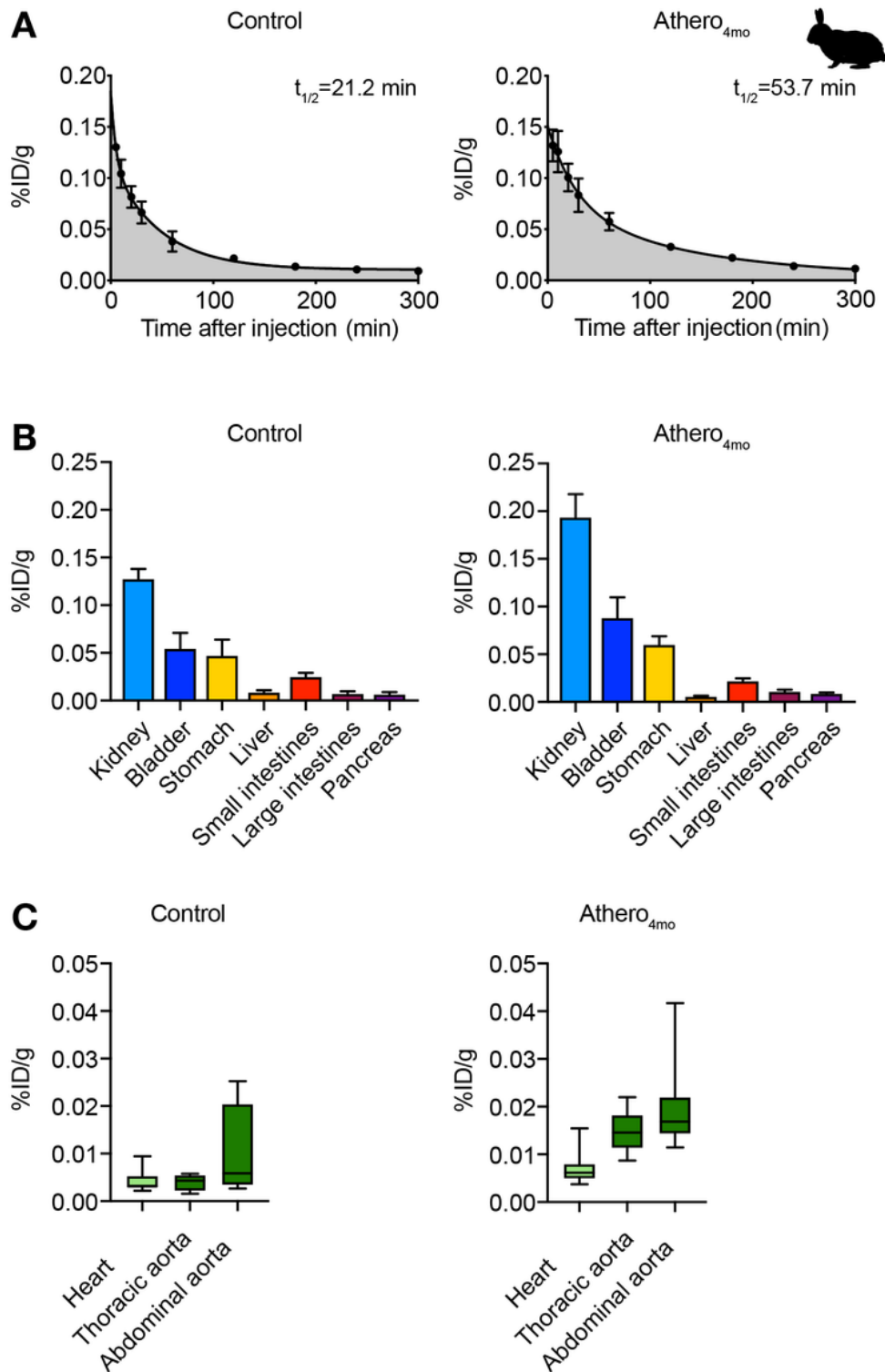


Figure 5

68Ga-DOTATATE pharmacokinetics and biodistribution in rabbits. A) Blood time-activity curve of 68Ga-DOTATATE-infused control (left) and athero4mo (right) rabbits. N=2-3 per time-point. Data are presented as mean \pm standard error of the mean. B) Ex vivo quantification of 68Ga-DOTATATE uptake in urinary and digestive organs of rabbits at 200 minutes after tracer injection, as determined by gamma counting. Data are presented as mean \pm standard error of the mean. C) Ex vivo quantification of 68Ga-DOTATATE uptake in the heart, thoracic and abdominal aorta 200 minutes after tracer injection, as determined by ex vivo gamma counting. N=6-9. Data are presented as median (interquartile range). ID: injected dose; t1/2: half-life.

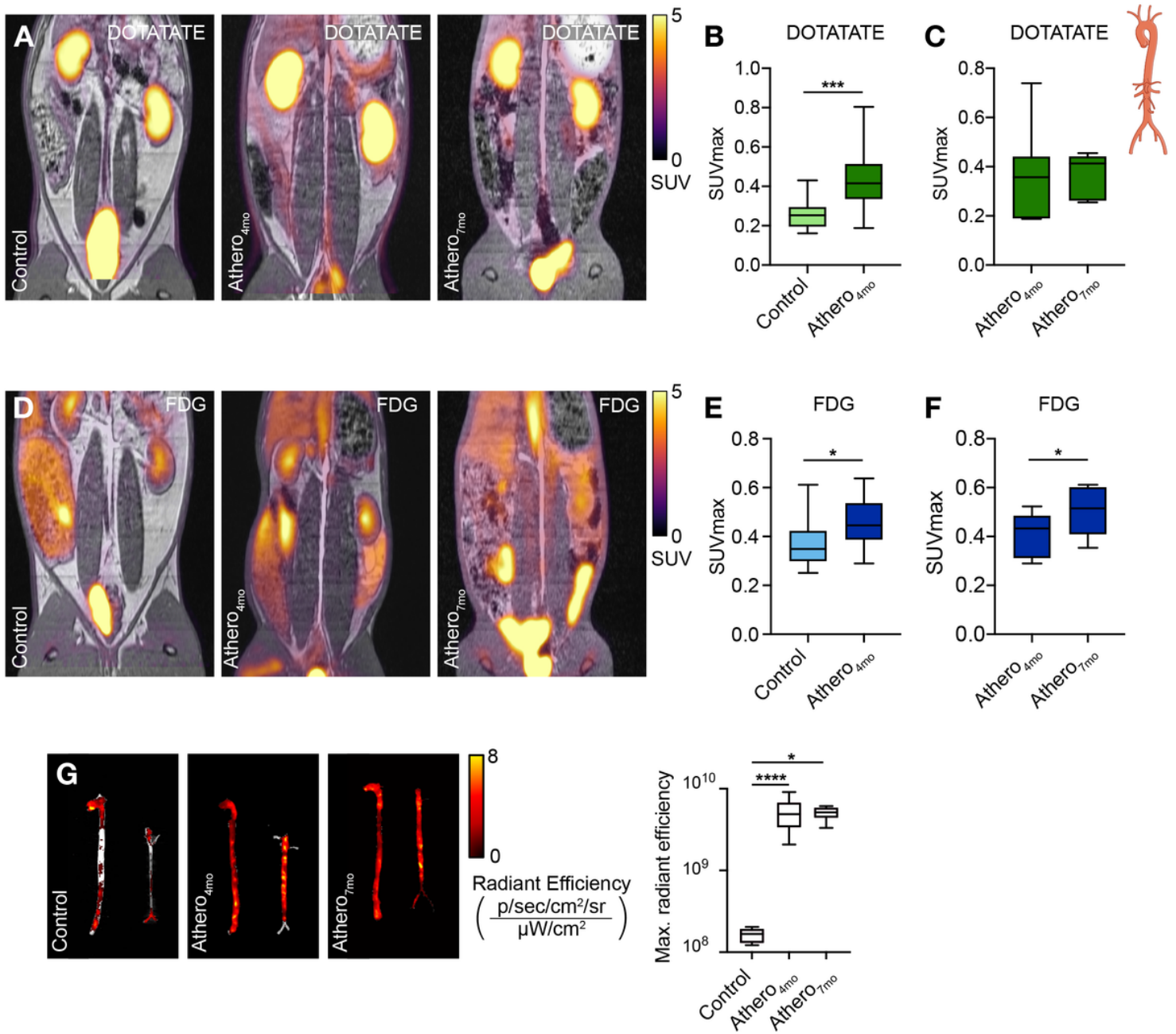


Figure 6

In vivo and ex vivo imaging of atherosclerosis in rabbits. A) Representative fused PET/MR image of ^{68}Ga -DOTATATE-infused control (left), athero4mo (middle) and athero7mo (right) rabbits. B) ^{68}Ga -DOTATATE SUVmax of abdominal aorta in control and athero4mo animals. N=10-32 per group. C) Paired analysis of ^{68}Ga -DOTATATE SUVmax of abdominal aorta in athero4mo and athero7mo animals. N=7. D) Representative fused PET/MR image of ^{18}F -FDG-infused control (left), athero4mo (middle) and athero7mo (right) rabbits. E) ^{18}F -FDG SUVmax of abdominal aorta in control and athero4mo animals. N=11-27 per group. F) Paired analysis of ^{18}F -FDG SUVmax of abdominal aorta in athero4mo and athero7mo animals. N=7 G) Near-infrared fluorescence imaging of Cy5.5-HDL in the aorta of rabbits. N=11-15 per group. DOTATATE: ^{64}Cu -DOTATATE; FDG: ^{18}F -FDG; SUVmax: maximum standardized uptake value. * $p < 0.05$, *** $p < 0.001$, **** $p < 0.0001$. Data are presented as median (interquartile range).

Supplementary Files

This is a list of supplementary files associated with this preprint. Click to download.

- [SupplementalDOTATATE101621SR.docx](#)
- [DOTAfigures101621YCTFigS1.pdf](#)
- [DOTAfigures101621YCTFigS2.pdf](#)
- [DOTAfigures101621YCTFigS3.pdf](#)
- [DOTAfigures101621YCTFigS4.pdf](#)